VORTEX RING RECONNECTIONS IN PARAXIAL LASER BEAMS

by

Zhamila Kulchukova

A Thesis Submitted to the Faculty of the

DEPARTMENT OF PHYSICS

In Partial Fulfillment of the Requirements
For the Degree of

BACHELOR OF SCIENCE

In the School of Sciences and Humanities

NAZARBAYEV UNIVERSITY

2023

NAZARBAYEV UNIVERSITY, SCHOOL OF SCIENCES AND HUMANITIES

As members of the thesis committee, we certify that we have read the thesis prepared by Zhamila Kulchukova entitled

VORTEX RING RECONNECTIONS IN PARAXIAL LASER BEAMS

and recommend that it be accepted as fulfilling the thesis requirement for the degree of Bachelor of Science.

Final approval and acceptance of this thesis is contingent upon the candidate's submission of the final copies of the thesis to the Department of Physics.

I hereby certify that I have read this thesis prepared under my direction and recommend that it be accepted as fulfilling the thesis requirement.

_____ Date: May 1, 2023

Thesis Director: Anton Desyatnikov

ABSTRACT

In recent years, optical vortex knots have been the subject of active research. The knots appear in various areas of physics and understanding the mechanism that is responsible for their formation is a problem that extends beyond optics. However, due to their spontaneous nature, it is impossible to predict their location. To unravel such a complex problem, it is important to understand simpler systems that may allow for the generation of vortex knots. In this thesis, I investigate the interference between the elliptical Gaussian beam and the plane wave, as a result of which vortex rings appear. The rings are basically the unknots, and the ellipticity allows for ring deformations. Consequently, at certain parameters, the rings are able to reconnect. I identify two types of ring reconnections: the reconnection that merges the rings together, and the self-crossing, where a loop-like structure is formed from a single ring crossing itself. This study has the potential to pinpoint specifics of the underlying mechanism that causes spontaneous knottings.

TABLE OF CONTENTS

1 INTRODUCTION

The 2008 Ig Nobel Prize winners proved that long strands of wire tumbled in a box would eventually tangle into knots [1]. Despite sounding so obvious, this finding raises an important question that is yet to be answered - what are the governing factors that cause knotting?

Knots appear in various nonlinear physical systems [2], from fluids to gravitational fields. In turbulence, one of the unsolved problems is the Navier-Stokes equation that describes the flow of fluids; knots that appear in the turbulent flow can describe the transport properties of plasma [3]. This concept is the basis of a recently emerged branch of physics - magnetohydrodynamics (also called topological fluid dynamics) [4].

The recent advancements in singular optics have also uncovered that optical vortices, lines of undefined phase, can be tied into knots [5, 6], and furthermore, they can even be observed in experiments [7, 8]. The light's ability to knot offers insight into its fine structure, deepening our understanding of its fundamental essence, which has been a topic of active research for centuries [9, 10]. However, due to their high sensitivity to perturbations, it is impossible to predict their exact location, nor what causes them to form [11].

Uncovering the underlying mechanisms of knotting is a difficult task due to the complexity of the system, and thus to understand it, we must foremost investigate simpler cases. In our research, we aim to identify a simpler system that generates the so-called unknots - vortex rings that can be manipulated into forming knot-like structures.

To better understand the context of this problem, it is essential to review the fundamental concepts first.

1.1 Lasers

The wave-like nature of light was uncovered a long time ago [12], which consequently laid the foundation for the development of lasers centuries later. Light Amplification by Stimulated Emission of Radiation, or laser in short, is a nonlinear device that emits a monochromatic coherent beam of light. The mechanism of the stimulated emission was predicted by A. Einstein [13], while the first ever laser was built by T. Maiman in 1960 [14] based on the theoretical work by A. Schawlow and C. Townes [15]. C. Townes also shared the 1964 Nobel Prize with N. Basov and A. Prokhorov [16] as the inventors of the laser and maser (laser in the microwave range) [17]. The maser was invented earlier than laser [18], and the frequency range was then extended to the visible and infrared ranges [19].

According to [15, 16], the laser consists of three main components: the energy source; the gain medium that emits light when excited; and the optical resonator consisting of two mirrors on the opposite sides of the gain medium, reflecting the light back and forth and transmitting the light of a specific frequency from one side. As a result, a

beam of photons of the same frequency and waveform is emitted, which is called the monochromatic coherent beam.

The laser beams can also be of various shapes and configurations, depending on the specific design of the optical resonator and the properties of the active medium [20]. For this thesis specifically, I focus on paraxial laser beams, which are the beams that propagate at small angles with respect to the optical axis. The beams of this type are very well collimated, meaning that they stay focused over long distances. The type of paraxial laser beam that we consider in our research has the Gaussian intensity profile and is thus called the Gaussian beam [21–23].

The Gaussian beam's intensity profile is described by the Gaussian function. The equation is derived through the paraxial wave equation (thus the name - paraxial laser beam) [24], and a more comprehensive description of the Gaussian beam is provided in chapter 2.

The Gaussian beams are extensively researched and find many applications in laser technology. One of the properties of the Gaussian beam that makes it useful in our research is that it is also widely used in forming optical vortices.

1.2 Optical vortices

The optical vortex is the topological structure, a line of undefined phase [25, 26]. They were first introduced as a new class of objects by J. Nye and M. Berry in 1974 [27], and the term "optical vortex" was proposed by P. Coullet, L. Gil and F. Rocca in 1989.

It is called a vortex because the light twists around the vortex line similar to vortices in water, and the number of twists done in one wavelength determines the topological charge of the vortex, which is an integer number. Since they are fundamentally a phase structure, vortices cannot be fully detected by analyzing the intensity profiles and intensity distributions alone [28]. They can be generated using a variety of techniques, such as directly encoding them into the laser or by twisting the light using materials and structures like holograms and crystals [29–32]. Optical vortices have been extensively studied in recent years, finding applications in areas of communication, imaging, cryptography, and many more [33, 34]. For example, optical tweezers [35], the invention of the 2018 Nobel Prize winner A. Ashkin that are used to capture small microscopic objects, are created through the use of optical vortices [36, 37]. The study of vortices gave rise to a new branch of physics known as singular optics [38].

The optical vortices can also be observed experimentally [39–41]. They were also extensively studied for their property to be tied into various intricate shapes, such as braids, rings, links, and knots, as mentioned [42], and the complexity of the structure is determined by the underlying physical system. Knots represent the most complex type of structure formed by optical vortices, and they can take on a variety of shapes, however, their spontaneous nature makes it difficult to predict their exact location [43, 44].

1.3 Motivation

Utilizing systems that generate unknots can be advantageous for understanding the underlying causes of knotting in complex systems. The recent work by A. Desyatnikov [45] describes a relatively simple system consisting of an interfering Gaussian beam and plane wave that results in the formation of unknots - vortex rings. The results are discussed in more detail in chapter 2.

For this thesis, I analyze the behavior of vortex rings that result from the interference of the elliptical Gaussian beam and the plane wave. The addition of ellipticity facilitates ring reconnections, a surprising result but a crucial step in the process of knot formation. First, I derive the equation describing the elliptical Gaussian beam and analyze its intensity iso-surfaces where the vortex rings appear. And since the optical vortices are phase structures, analyzing the phase profile of the interference results in the exact locations of the vortex rings. The ellipticity of the beam deforms the rings, which allows me to pinpoint the specific parameters which cause ring reconnections. There are two specific types of reconnections identified: the reconnections that merge rings together; and self-crossings, where a single ring crosses itself forming a loop-like structure.

The next step would be to introduce the rotating beam and investigate if it has any effect on knot formation, however, this is the work for further research. In this thesis, the focus is on reconnections only.

Although no knots are tied within the extent of this thesis, the fact that ring reconnections can be observed in a simple system indicates that we are making progress in unraveling the mystery of knotting.

2 MODEL AND BACKGROUND

This section provides the necessary mathematical background for the topic. The paraxial wave equation is derived first and the equation describing the electric field of the Gaussian beam is presented in more detail. Furthermore, this section includes a review of the paper that presents the vortex rings resulting from the interference of a radially symmetric beam and a plane wave, which serves as the basis for my research.

2.1 Paraxial wave equation

Paraxial laser beams are well-collimated beams, meaning that they spread minimally as they propagate. Such beams are governed by the paraxial approximation of the Helmholtz equation [46, 47].

Starting with Maxwell's equations:

$$\begin{aligned} \nabla \cdot \mathbf{E} &= \frac{\rho}{\epsilon_0} \\ \nabla \times \mathbf{E} &= -\frac{\partial \mathbf{B}}{\partial t} \\ \nabla \cdot \mathbf{B} &= 0 \\ \nabla \times \mathbf{B} &= \mu_0 \left(\mathbf{J} + \epsilon_0 \frac{\partial \mathbf{E}}{\partial t} \right) \end{aligned} \tag{2.1}$$

We consider a beam in free space, so the presence of charge ρ and flux $\mathbf{J}$ densities is omitted, which results in the following set of equations:

$$\nabla \cdot \mathbf{E} = 0 \tag{2.2a}$$

$$\nabla \times \mathbf{E} = -\frac{\partial \mathbf{B}}{\partial t} \tag{2.2b}$$

$$\nabla \cdot \mathbf{B} = 0 \tag{2.2c}$$

$$\nabla \times \mathbf{B} = \mu_0 \epsilon_0 \frac{\partial \mathbf{E}}{\partial t} \tag{2.2d}$$

It is now possible to obtain the Helmholtz equation using eq. (2.2b) and eq. (2.2d).

$$\begin{aligned} \nabla \times (\nabla \times \mathbf{E}) &= \nabla \times \left(-\frac{\partial \mathbf{B}}{\partial t} \right) \\ \nabla \times (\nabla \times \mathbf{B}) &= \nabla \times \left(\mu_0 \epsilon_0 \frac{\partial \mathbf{E}}{\partial t} \right) \end{aligned}$$

The left-hand side of the equations can be expanded as $\nabla(\nabla \cdot \mathbf{X}) - \nabla^2 \mathbf{X}$, where $\mathbf{X}$ is either $\mathbf{E}$ or $\mathbf{B}$. The first term $\nabla(\nabla \cdot \mathbf{X})$ is 0 for both cases, which is a consequence of eq. (2.2a) and eq. (2.2c). The right-hand side expands into the following: $\nabla \times \left(\frac{\partial \mathbf{X}}{\partial t}\right) = \frac{\partial}{\partial t}(\nabla \times \mathbf{X})$. Substituting eq. (2.2b) and eq. (2.2d) into $\nabla \times \mathbf{X}$, the Helmholtz equations

can be obtained:

$$\nabla^2\mathbf{E} - \mu_0\epsilon_0\frac{\partial^2\mathbf{E}}{\partial t^2} = 0$$
$$\nabla^2\mathbf{B} - \mu_0\epsilon_0\frac{\partial^2\mathbf{B}}{\partial t^2} = 0$$

Now we consider a monochromatic beam approximation. Although the "true" monochromatic beam does not exist - the laser emits a very narrow range of frequencies, using the monochromatic approximation still yields a valid result. The time-dependent factor $\exp(-i\omega t)$ and the scalar spatial part $\mathcal{E}$ and $\mathcal{B}$ can be separated.

$$\mathbf{E} = \mathrm{Re}[\boldsymbol{\mathcal{E}}\exp(-i\omega t)] \qquad\qquad \mathbf{B} = \mathrm{Re}[\boldsymbol{\mathcal{B}}\exp(-i\omega t)] \tag{2.5}$$

Using the given approximation in eq. (2.5) and introducing wavenumber parameter $k = \omega\sqrt{\mu_0\epsilon_0}$, the Helmholtz equation for $\boldsymbol{\mathcal{E}}$ and $\boldsymbol{\mathcal{B}}$ is obtained:

$$\begin{aligned}\nabla^2\boldsymbol{\mathcal{E}} - k^2\boldsymbol{\mathcal{E}} = 0\\ \nabla^2\boldsymbol{\mathcal{B}} - k^2\boldsymbol{\mathcal{B}} = 0\end{aligned} \tag{2.6}$$

Recalling the properties of paraxial laser beams, assuming that the propagation is in z-direction, the largest component of the wavevector $\mathbf{k} = k_x\hat{\mathbf{x}} + k_y\hat{\mathbf{y}} + k_z\hat{\mathbf{z}}$ must be k_z. Thus, the paraxial approximation requires the following:

$$k_z = \sqrt{k^2 - k_x^2 - k_y^2} \approx k - \frac{k_x^2 + k_y^2}{2k} \tag{2.7}$$

Now we consider the solution of eq. (2.6) which explicitly depends on $\exp(ikz)$ with amplitude distribution $u(\mathbf{r})$:

$$\mathcal{E}(\mathbf{r}) = E(\mathbf{r})\exp(ikz) \tag{2.8}$$

Substituting eq. (2.8) into eq. (2.6) and employing the paraxial approximation $\left|\frac{\partial^2 E}{\partial z^2}\right| \ll k\left|\frac{\partial E}{\partial z}\right|$ will result in the the paraxial wave equation u:

$$\Delta E + 2ik\frac{\partial E}{\partial z} = 0, \tag{2.9}$$

where the operator Δ is the Laplace operator in two dimensions: $\Delta = \frac{\partial^2}{\partial x^2} + \frac{\partial^2}{\partial y^2}$.

The paraxial wave equation has many solutions. As mentioned, for this thesis I am using the solution describing the Gaussian beam specifically, on which I will elaborate in the following subchapter.

2.2 Gaussian beams

One of the types of solutions to eq. (2.9) is the Gaussian beam, which has the Gaussian intensity profile. The Hermite-Gaussian (HG) and Laguerre-Gaussian (LG) modes are two complete sets of solutions, one arising from systems with rectangular symmetry and the other from systems with radial symmetry respectively.

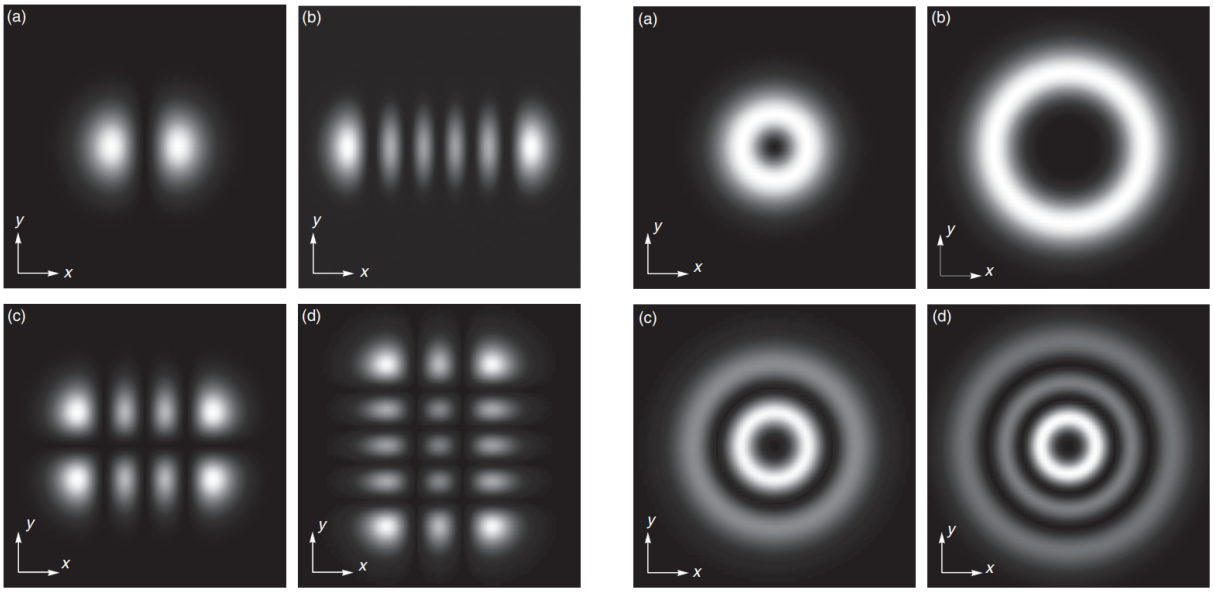

(a) Hermite-Gaussian modes (b) Laguerre-Gaussian modes

Figure 1: The example plots for intensity profiles of four HG and LG beams. For both, (a) $n = 1, m = 0$ and (b) $n = 5, m = 0$. In a (c) $n = 3, m = 1$ and (d) $n = 2, m = 4$, while in b (c) $n = 2, m = 1$, (d) $n = 2, m = 2$. Images taken from [46].

$$\begin{aligned}\mathcal{E}_{nm}^{HG}(x,y,z) =& E_0 \frac{w_0}{w(z)} H_n\left(\frac{x\sqrt{2}}{w(z)}\right) \exp\left(-\frac{x^2}{w^2(z)}\right) H_m\left(\frac{y\sqrt{2}}{w(z)}\right) \exp\left(-\frac{y^2}{w^2(z)}\right) \\ &\times \exp\left(ik\frac{x^2+y^2}{2R(z)} - i(1+n+m)\arctan\frac{z}{z_R}\right)\end{aligned} \tag{2.10a}$$

$$\begin{aligned}\mathcal{E}_{nm}^{LG}(r,\theta,z) =& E_0 \frac{w_0}{w(z)} \left(\frac{r\sqrt{2}}{w(z)}\right)^{|n|} \exp\left(-\frac{r^2}{w^2(z)}\right) L_m^{|n|}\left(\frac{2r^2}{w^2(z)}\right) \exp\left(in\theta\right) \\ &\times \exp\left(ik\frac{r^2}{2R(z)} - i(1+|n|+2m)\arctan\frac{z}{z_R}\right)\end{aligned} \tag{2.10b}$$

Here, $w(z)$ is the function of the beam radius where the amplitude falls to $1/e$ of its value on the axis of propagation and w_0 is the spot size of the beam. $R(z)$ is the radius of the curvature of the beam's wavefront and z_R is the so-called Rayleigh range - the distance along the propagation direction between the waist and the point where the cross-section of the beam doubles. The terms $\arctan\frac{z}{z_R}$ is also called Gouy phase which attributes to the phase velocity. The terms n and m are integers, and H_m and $L_m^{|n|}$ depict

the Hermite and Laguerre polynomials respectively (hence the names - Hermite-Gaussian and Laguerre-Gaussian).

The shape of the beam is defined by the waist w_0 and wavenumber k.

$$z_R = \frac{\pi w_0^2}{\lambda} = \frac{1}{2} k w_0^2 \tag{2.11a}$$

$$w(z) = w_0 \sqrt{1 + \left(\frac{z}{z_R}\right)^2} \tag{2.11b}$$

$$R(z) = z \left[1 + \left(\frac{z_R}{z}\right)^2\right] \tag{2.11c}$$

Both of the modes at $n = 0$ and $m = 0$ produce a single round spot similar to what we expect to get from lasers. The said mode is called the fundamental Gaussian beam and is given in the following form:

$$\mathcal{E}(r, z) = E_0 \frac{w_0}{w(z)} \exp\left(-\frac{r^2}{w(z)}\right) \exp\left(ik\frac{r^2}{2R(z)} - i \arctan\frac{z}{z_R}\right) \tag{2.12}$$

Now, using the scaling properties of the system, the dimensionless transverse variables (x, y, t) are introduced and derived from the dimensional variables $(\tilde{x}, \tilde{y}, \tilde{z})$ in the following manner: $x = \tilde{x}/w_0$, $y = \tilde{y}/w_0$, $t = \tilde{z}/z_R$ and $\kappa = k z_R$. The amplitude E_0 is normalized to 1. This will transform the equations governing the shape of the beam in eq. (2.11) into:

$$w(t) = \sqrt{1 + t^2} \tag{2.13a}$$

$$R(t) = \frac{1}{t}\left(1 + t^2\right) \tag{2.13b}$$

Consequently, the Schrödinger-type paraxial wave equation in eq. (2.9) describing the amplitude of the beam is modified to the following form:

$$4i\frac{\partial E}{\partial t} + \frac{\partial^2 E}{\partial x^2} + \frac{\partial^2 E}{\partial y^2} = 0 \tag{2.14}$$

From here on, the equations will be denoted in dimensionless coordinates.

2.3 Vortex rings

This subchapter is a review of an unpublished article by A. Desyatnikov (2023) on vortex rings formed as a result of interference of the Gaussian laser beam and a plane wave [45].

The ansatz is of a familiar form: $\mathcal{E}(x, y, t) = E(x, y, t) \exp(i\kappa t)$, where $|E(x, y, t)|$ is the amplitude distribution and the phase is $\arg E = \psi(x, y, t) + \alpha$. Here, α is an arbitrary phase constant.

The final equation of the beam in cylindrical coordinates is as follows:

$$E(r,t) = \frac{1}{\sqrt{1+t^2}} \exp\left(-\frac{r^2}{1+t^2} + i\psi(r,t)\right), \tag{2.15}$$

where the phase ψ is:

$$\psi(r,t) = \frac{r^2 t}{1+t^2} - \arctan t, \tag{2.16}$$

This equation is the dimensionless version of the fundamental Gaussian beam mode described in eq. (2.12).

The following superposition with a plane wave is considered:

$$\mathcal{E} = E(r,t)e^{i\kappa t + i\alpha} + Pe^{i\kappa_1 t + i\beta} \tag{2.17}$$

Here, P is the relative amplitude of the plane wave, and β is the arbitrary phase constant similar to α in $\mathbf{E}(r,t)$. κ_1 is the dimensionless wavenumber for the plane wave.

Recalling chapter 1, it is impossible to obtain vortices by only investigating the zero intensity lines on the field, so to find the vortices, both the amplitude of the field and the phase must be analyzed.

The field zeros appear at the intersection of two surfaces:

$$\operatorname{Re}\mathcal{E} = 0 : |E(r,t)| = P \tag{2.18a}$$

$$\operatorname{Im}\mathcal{E} = 0 : \psi(r,t) + (\kappa - \kappa_1)t = \phi + 2\pi n \tag{2.18b}$$

In eq. (2.18b), parameter ϕ is defined as the phase difference $\phi = \pi + \beta - \alpha$. In case of co-propagating plane wave, $\kappa = \kappa_1$, and so the term $(\kappa - \kappa_1)t$ in eq. (2.18b) vanishes. In this thesis, I only consider the case of co-propagation.

The equation (2.18a) describes the surface of constant intensity where the rings are located. The solution to the equation is given in the form of spheroids - enclosed surfaces in three dimensions that resemble a deformed sphere. Solving for r in eq. (2.18a) and defining $\rho(t) = r$, the mathematical form of the spheroids is obtained:

$$\rho(t) = \sqrt{-(1+t^2)\ln\left(P\sqrt{1+t^2}\right)} \tag{2.19}$$

The spheroids in eq. (2.19) can be classified into two distinct shapes: a simple one with a maximum at $t = 0$ and a dumbbell-like with a minimum at $t = 0$ and two maxima at $t = \pm\frac{1}{\sqrt{P^2(e-1)}}$.

By substituting eq. (2.19) into eq. (2.18b), the equation for the phase at the spheroids can be obtained:

$$\psi_0(\rho,t) = -t\ln\left(P\sqrt{1+t^2}\right) - \arctan t = \phi + 2n\pi \tag{2.20}$$

Solving for a parameter ϕ, the values of t in eq. (2.20) denote the locations of the rings along the direction of propagation.

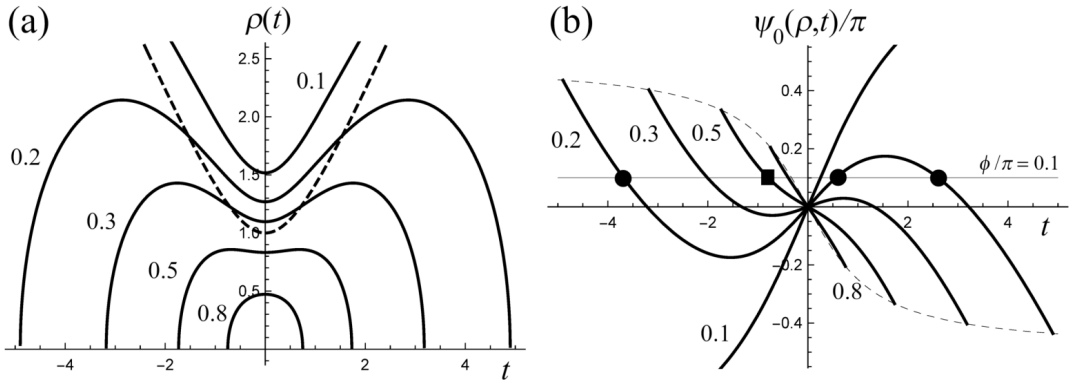

Figure 2: Equations for spheroids eq. (2.19) and phase at the spheroids eq. (2.20) plotted for various values of relative amplitude P (0.1, 0.2, 0.3, 0.5, 0.8). Images taken from [45].

At large relative amplitude P, specifically $P > 1/e$, only one ring appears. At $P < 1/e$, more rings will appear and their amount is predicted by the number of roots in eq. (2.20).

The following plots are an example of the resulting vortex rings:

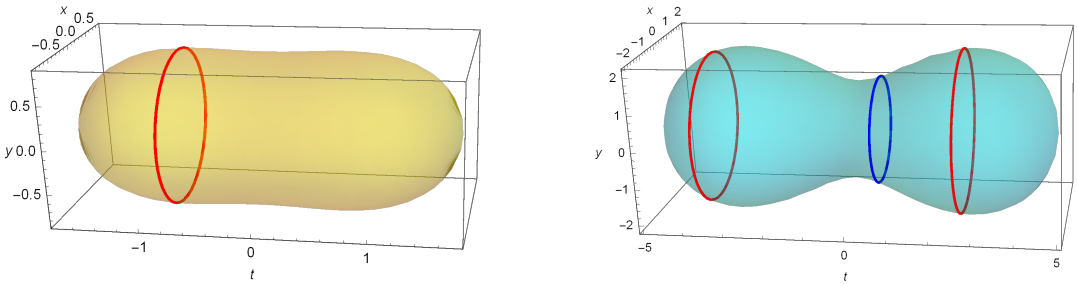

(a) $P = 0.5$ (b) $P = 0.2$

Figure 3: The vortex rings formed as a result of the interference of the radially symmetric Gaussian beam and the co-propagating plane wave. The red rings rotate in the opposite direction relative to the blue ring.

The rings inside the so-called half-width hyperboloid $\rho < \sqrt{1+t^2}$ are of opposite topological charge relative to the rings outside, meaning they rotate in the opposite direction.

The rings in this setup appear via two mechanisms: nucleation, where a vortex ring collapses into a single point, and annihilation, where two rings of opposite topological charge merge and cancel each other out. In fig. 3a, the single ring nucleates from a single point along the optical axis, which corresponds to either of the endpoints of the spheroid. In fig. 3b however, both of the mechanisms take place: the rings nucleate at the endpoints $\rho = 0$ and annihilate at $\rho = \sqrt{1+t^2}$.

The vortex rings obtained via this setup are perfectly round and preserve their shape as the phase difference ϕ varies. Because of their rigid shape, no reconnections are possible, since the moment the rings touch each other will cause them to annihilate. However,

this is not the case for the elliptical beams, where the ellipticity introduces additional perturbation that deforms the rings in various ways. This phenomenon is investigated in more detail in the next chapter.

3 VORTEX RINGS AND RING RECONNECTIONS

This section outlines the findings of my study. First, I derive the equation describing the elliptical Gaussian beam and consider the same interference problem as in eq. (2.17). It is important to note that I derive the equation for the rotating elliptical beam. Although rotations are not unitized in the scope of this thesis, it provides the basis for future research into knot formations, which is why the equation is only mentioned here.

The vortex rings appear similar to fig. 2.3, however, depending on the ellipticity of the beam, the rings are deformed to various degrees. Moreover, I present that at a very specific set of parameters P, ϕ and ellipticity ϵ, the rings can be reconnected and self-crossed.

3.1 Elliptical Gaussian beams

The elliptical Gaussian beam has different waist sizes w_0 in x- and y-directions, and thus, different diffraction rates that are dictated by the beam parameters described in eq. (2.11).

$$z_{Rx} = \frac{1}{2}kw_{0x}^2 \qquad z_{Ry} = \frac{1}{2}kw_{0y}^2 \tag{3.1a}$$

$$w_x(z) = w_{0x}\sqrt{1+\left(\frac{z}{z_{Rx}}\right)^2} \qquad w_y(z) = w_{0y}\sqrt{1+\left(\frac{z}{z_{Ry}}\right)^2} \tag{3.1b}$$

$$R_x(z) = z\left[1+\left(\frac{z_{Rx}}{z}\right)^2\right] \qquad R_y(z) = z\left[1+\left(\frac{z_{Ry}}{z}\right)^2\right] \tag{3.1c}$$

To avoid the loss of generality and for the sake of convenience, the dimensionless transverse parameters defined in section 2.3 need to be applied to eq. (3.1). However, since there are two different waist radii w_{0x} and w_{0y}, there are twice as many beam parameters to deal with. To resolve this issue, I introduce an additional parameter ϵ that describes the ellipticity of the beam:

$$w_{0x} = \sqrt{2}\cos\epsilon \qquad w_{0y} = \sqrt{2}\sin\epsilon \tag{3.2}$$

The term $\sqrt{2}$ appears as a normalization factor; at $\epsilon = \pi/4$, which is the ellipticity parameter for a radially symmetric beam, w_{0x} and w_{0y} must be equal to exactly 1. At $0 < \epsilon < \pi/4$, the waist radius w_{0x} will be larger than w_{0y}, so the beam will appear elongated along x-axis; for $\pi/4 < \epsilon < \pi/2$, the beam will appear elongated along y-axis. Now applying eq. (3.2) to eq. (3.1a), I parametrize the Rayleigh ranges z_{Rx} and z_{Ry}:

$$z_{Rx} = 2\cos^2\epsilon \qquad z_{Ry} = 2\sin^2\epsilon \tag{3.3}$$

Applying both the dimensionless coordinates $t = z/z_R$ and the parametrized waist radii in eq. (3.2), I obtain the following functions of spot size and radius of the curvature

from eq. (3.1b) and eq. (3.1c):

$$w_x(t) = \frac{w_0}{2\cos\epsilon}\sqrt{8\cos^4\epsilon + 2t^2} \qquad w_y(t) = \frac{w_0}{2\sin\epsilon}\sqrt{8\sin^4\epsilon + 2t^2} \tag{3.4a}$$

$$R_x(t) = \frac{z_R}{t}\left(4\cos^4\epsilon + t^2\right) \qquad R_y(t) = \frac{z_R}{t}\left(4\sin^4\epsilon + t^2\right) \tag{3.4b}$$

Now I derive the equation for the fundamental elliptical Gaussian beam in transverse dimensionless coordinates. To do so, I am solving the same Schrödinger-type paraxial wave equation as in eq. (2.14) and introduce the ansatz:

$$E(x,y,t) = A(t)\exp\left(-\left[\frac{X^2}{a(t)} + \frac{Y^2}{b(t)}\right] + i\psi(X,Y,t)\right) \tag{3.5}$$

Here, X, Y are a new principal coordinate system that allows me to introduce rotation. Coordinates $\{X, Y\}$ are simply $\{x, y\}$ rotated by the angle θ in the following manner:

$$\begin{bmatrix} X \\ Y \end{bmatrix} = \begin{bmatrix} \cos\theta & -\sin\theta \\ \sin\theta & \cos\theta \end{bmatrix}\begin{bmatrix} x \\ y \end{bmatrix} = \begin{bmatrix} x\cos\theta - y\sin\theta \\ x\sin\theta + y\cos\theta \end{bmatrix} \tag{3.6}$$

Variable θ introduces an additional degree of freedom; at fixed θ the beam is non-rotating, but by varying θ in time, the rotation of the beam can be introduced.

Solving for the eq. 2.14 by using the ansatz in eq. (3.5), I obtain the equation of the rotating elliptical beam (more details will be added later):

$$\begin{aligned} E(x,y,t) = {} & \frac{\sin 2\epsilon}{\left[(4\cos^4\epsilon + t^2)(4\sin^4\epsilon + t^2)\right]^{1/4}} \\ & \times \exp\left[-\left(\frac{\cos^2\theta}{w_x^2(t)} + \frac{\sin^2\theta}{w_y^2(t)}\right)x^2 - \left(\frac{\sin^2\theta}{w_x^2(t)} + \frac{\cos^2\theta}{w_y^2(t)}\right)y^2 - \left(\frac{\sin 2\theta}{w_y^2(t)} - \frac{\sin 2\theta}{w_x^2(t)}\right)xy\right] \\ & \times \exp\left[i\left(\frac{\cos^2\theta}{R_x(t)} + \frac{\sin^2\theta}{R_y(t)}\right)x^2 + i\left(\frac{\sin^2\theta}{R_x(t)} + \frac{\cos^2\theta}{R_y(t)}\right)y^2 + i\left(\frac{\sin 2\theta}{R_y(t)}\cdot\frac{\sin 2\theta}{R_x(t)}\right)xy\right] \\ & \times \exp\left[-\frac{i}{2}\left(\arctan\left[\frac{t}{2\cos\epsilon^2}\right] + \arctan\left[\frac{t}{2\sin\epsilon^2}\right]\right)\right] \end{aligned} \tag{3.7}$$

To reiterate, this equation describes the rotating elliptical beam, although not used, it is important for future investigation.

3.2 Vortex rings and deformations

For this thesis, I investigate the interference of a non-rotating stigmatic beam and a co-propagating plane wave, which should result in vortex rings being formed.

Since the beam is non-rotating, I can set $\theta = 0$, which simplifies the beam equation

(3.7):

$$E(x,y,t) = \frac{\sin 2\epsilon}{\left[(4\cos^4\epsilon + t^2)(4\sin^4\epsilon + t^2)\right]^{1/4}} \times \exp\left[-\frac{x^2}{w_x^2(t)} - \frac{y^2}{w_y^2(t)} + i\left(\frac{x^2}{R_x(t)} + \frac{y^2}{R_y(t)}\right)\right] \times \exp\left[-\frac{i}{2}\left(\arctan\left[\frac{t}{2\cos\epsilon^2}\right] + \arctan\left[\frac{t}{2\sin\epsilon^2}\right]\right)\right]$$

Now solving for the real and imaginary parts in eq. (2.18), I obtain the following two equations:

$$\frac{\sin 2\epsilon}{\left[(4\cos^4\epsilon + t^2)(4\sin^4\epsilon + t^2)\right]^{1/4}} \exp\left[-\frac{2x^2\cos^2\epsilon}{4\cos^4\epsilon + t^2} - \frac{2y^2\sin^2\epsilon}{4\sin^4\epsilon + t^2}\right] = P \tag{3.8}$$

$$\frac{x^2 t}{4\cos^4\epsilon + t^2} + \frac{y^2 t}{4\sin^4\epsilon + t^2} - \frac{1}{2}\left(\arctan\left[\frac{t}{2\cos\epsilon^2}\right] + \arctan\left[\frac{t}{2\sin\epsilon^2}\right]\right) = \phi + 2\pi n \tag{3.9}$$

The equation (3.8), similar to that of eq. (2.19), describes the intensity iso-surfaces (spheroids) on which the rings are located. But unlike eq. (2.19), where it was possible to easily solve for r, this equation will remain in an implicit form. The same applies to eq. (3.9), which describes the phase at the spheroids. However, this still allows me to numerically solve for the intersection of the two surfaces eq. (3.8) and eq. (3.9), and vortex rings will be obtained.

Spheroids in eq. (3.8) are elliptically deformed, so their shape will be highly dependent on the parameter ϵ in addition to the relative intensity P. By varying P and ϵ, spheroids of different shapes will be obtained, as plotted in the figures below.

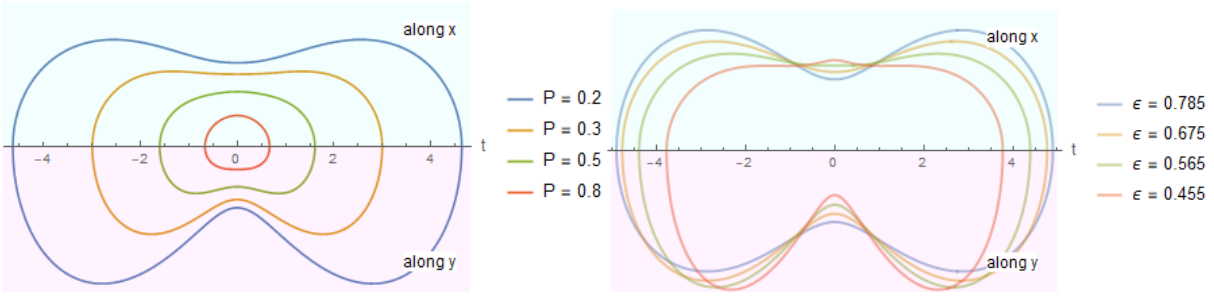

(a) Varying intensity ($\epsilon = 0.628$) (b) Varying ellipticity ($P = 0.2$)

Figure 4: Shapes of the spheroids change as as the parameters P and ϵ vary. The upper and lower parts of the figures represent the intersection curves of the spheroids with xt and yt planes respectively. (a) Spheroids of intensity $P = 0.2, P = 0.3, P = 0.5$ and $P = 0.8$. (b) Spheroids of ellipticity $\epsilon = 0.455, \epsilon = 0.565, \epsilon = 0.675$ and $\epsilon = 0.785$, the latter represents the shape for a radially symmetric beam.

It is important to note that the ellipticity parameter ϵ depicts the deformation relative to the radially symmetric beam $\epsilon = \pi/4 \approx 0.785$ since the shape of the beam deforms

depending on $\sin\epsilon$ and $\cos\epsilon$. At $\sin\epsilon = \cos\epsilon$, the beam is radially symmetric; at $\sin\epsilon < \cos\epsilon$, which is the interval $(0, \pi/4)$, the beam is elongated along x-axis at $t = 0$, and at $\sin\epsilon > \cos\epsilon$, $(\pi/4, \pi/2)$, the beam is elongated along y-axis. Due to the symmetry of $\sin\epsilon$ and $\cos\epsilon$ functions, the spheroids of intensity P, phase ϕ and ellipticity $\epsilon = \pi/4 \pm \epsilon_0$ will be of the same shape and behave in the same way despite being elongated along different axes.

The extent of the spheroids can be calculated by setting $x = 0$ and $y = 0$ and evaluating the resulting equation $(t^2 - \sin^2 2\epsilon)^2 + 4t^2 = P^{-4}\sin^4 2\epsilon$ for the set of parameters $\{\epsilon, P\}$. Furthermore, from figure 4a it can be noticed that the curves can either have a maximum or a minimum point at $t = 0$, with the latter resulting in the dumbbell-like shape. The smaller P gets, the more dumbbell-like the shape gets. The shapes are sensitive to ϵ, as can be seen from figure 4b.

The following are the spheroids plotted in 3D:

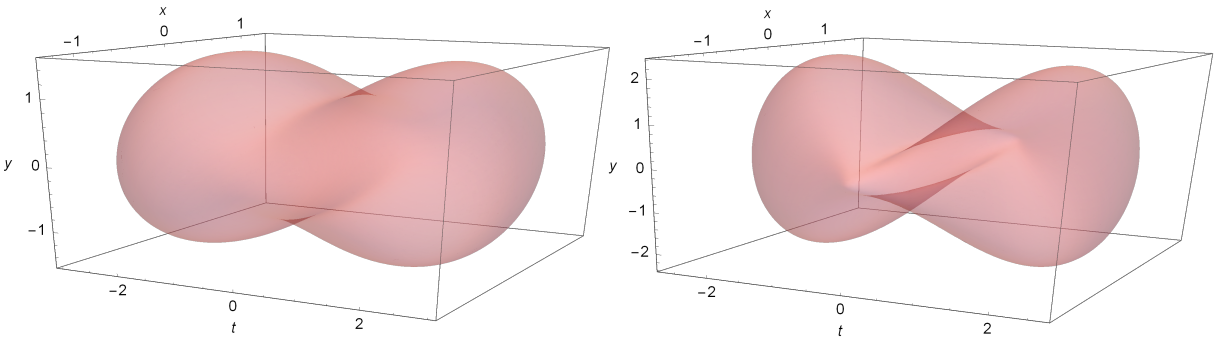

(a) $\epsilon = 0.628$ (b) $\epsilon = 0.314$

Figure 5: Spheroids of the same intensity but different ellipticity, $P = 0.3$.

As expected, the spheroid in fig. 5b is more elongated along the x-axis compared to the one in fig. 5a. When looked into more closely, the "spikes" facing outwards along $x-$axis at $t = 0$ on 5b can also be noticed, which appear due to a very large difference between the diffraction rates at x- and y-directions. The same can be seen in fig. 4b, the shape of the $\epsilon = 0.456$ curve has a visible spike along $x-$axis compared to the other curves with milder ellipticity. At $\epsilon = 0$ and $\epsilon = \pi/2$, the beam collapses and no spheroids are possible to be produced.

Substituting the equation for the spheroids eq. (3.8) into eq. (3.9), the resulting phase equation is obtained:

$$\begin{aligned} &-\frac{t}{8}\left(\frac{x^2(4\sin^4\epsilon + t^2) + y^2(4\cos^4\epsilon + t^2)}{x^2\cos^2\epsilon(4\sin^4\epsilon + t^2) + y^2\sin^2\epsilon(4\cos^4\epsilon + t^2)}\right)\cdot \\ &\cdot \ln\left[P^4\frac{(4\cos^4\epsilon + t^2)(4\sin^4\epsilon + t^2)}{\sin^4 2\epsilon}\right] - \\ &-\frac{1}{2}\left(\arctan\left[\frac{t}{2\cos^2\epsilon}\right] + \arctan\left[\frac{t}{2\sin^2\epsilon}\right]\right) = \phi \end{aligned} \tag{3.10}$$

ϕ is the phase difference that varies from $(-\pi, \pi)$, it will now be possible to locate the rings. The rings appear at the intersection of eq. (3.8) and eq. (3.9), therefore, combining them graphically will result in rings being formed at the surface of spheroids as presented in the figure below:

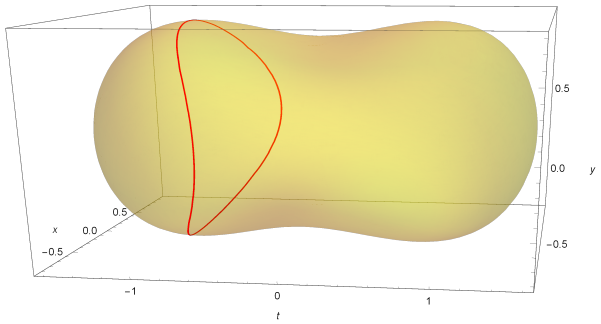

Figure 6: The vortex ring on spheroids for parameters $\epsilon = 0.628$, $P = 0.5$ and $\phi = 0.314$.

In comparison to fig. 2.3, the ring is deformed towards the center at the plane $y = 0$. This is due to the difference in diffraction rates at the x- and y- directions, which results in deformation depending on the chosen ϵ and ϕ. It might seem like the ring curves towards the center, but in fact, it curves outwards, since the larger diffraction rate at one of the axis "drags" the rings outwards. In this case, $\epsilon = 0.628 < 0.785$ (ellipticity of the radially symmetric beam) means that the diffraction rate is higher along the $y-$axis, so the ring is curved outwards at $x = 0$.

Now I consider the case where three vortex rings appear, plotted as below:

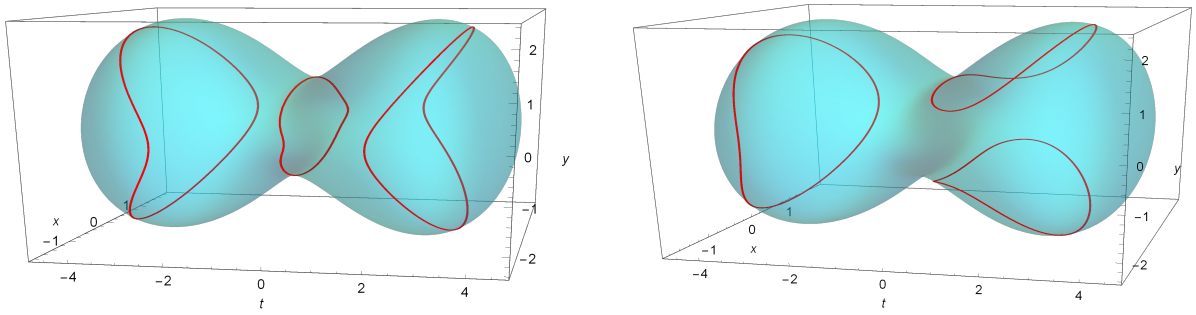

(a) $\phi = 0.031$ (b) $\phi = 0.314$

Figure 7: Vortex rings on spheroids for parameters $\epsilon = 0.628$ and $P = 0.2$. a Three separate rings deformed outwards along the axis of higher diffraction rate. In this case, the diffraction rate is higher along y. b Three separate rings, but the two rings on the right are located above and below the t-axis.

Surprisingly, the rings in fig. 7b appear to be located below and above the t-axis, unlike the rings in fig. 7a, which are, as expected, located along the t-axis deforming at y-direction. In fact, the phenomenon shown in fig. 7b can also be explained by the

difference in diffraction rates - after the certain threshold value of ϕ, the rings get dragged outwards along the axis of higher diffraction rate.

Examining the shapes of the rings more closely, at lower ϕ, the two rings on the right side of the spheroid are deforming towards the point in-between them on the $y = 0$ plane. As ϕ increases, it appears as if rings continue to deform towards each other until they reconnect and "merge" at a certain ϕ and then get divided into two separate rings that are located above and below the t-axis, as presented in fig. 7b. So it should be expected that by tuning ϕ for the given ϵ and P recovering the picture with rings reconnecting at a certain point t will be possible.

By further observing rings for different parameters, at a slightly higher ellipticity and ϕ close to 0, the ring on the left side of the beam appears to self-cross, bending towards the origin, as presented in the figure below:

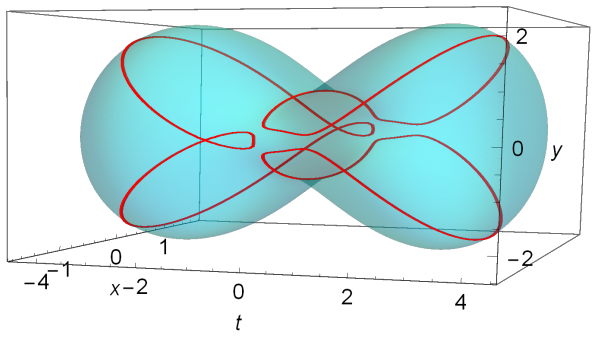

Figure 8: The self-crossing vortex ring resulted from the parameters $\epsilon = 0.571$, $P = 0.2$ and $\phi = 0.0041$.

Even though I say it is "bent towards the origin", in fact, the high ellipticity of $\epsilon = 0.571$ means that the ring deformation is more severe, which results in a ring's edges dragging further outwards than it appears to be for milder ellipticities.

The self-crossing of the ring is a phenomenon that was not expected to be retrieved. Furthermore, there is not a single simple justification for the ring to behave in this way. Despite not having a ground for explaining this phenomenon, the fact that it happens in a relatively simple system with a stigmatic elliptical beam and a plane wave is quite intriguing.

Noting all of the above, by tracing a very specific set of parameters $\{\epsilon, P, \phi\}$, the vortex ring reconnections and self-crossings can be predicted.

3.3 Reconnections and self-crossings

Figure 7a demonstrates that the ring reconnections and self-crossings likely happen at $y = 0$ for $\epsilon < 0.785$ and at $x = 0$ for $\epsilon > 0.785$. Setting $y = 0$ in eq. (3.9) results in the equation that represents the phase at the plane $y = 0$:

$$\psi_0(t,\epsilon) = -\frac{t}{(2\cos^2\epsilon)}\ln\left[P^4\frac{(4\cos^4\epsilon+t^2)(4\sin^4\epsilon+t^2)}{\sin^4 2\epsilon}\right] - \\ -\frac{1}{2}\left(\arctan\left[\frac{t}{2\cos^2\epsilon}\right]+\arctan\left[\frac{t}{2\sin^2\epsilon}\right]\right) \tag{3.11}$$

I know a-posteriori that the reconnections and self-crossings happen at the parameters that represent the coordinates of extremum points of eq. (3.11). Obtaining them requires finding the extremum values of ψ_0 and setting them equal to ϕ. Plotting the said equation directly for $P = 0.2$ results in the following diagram:

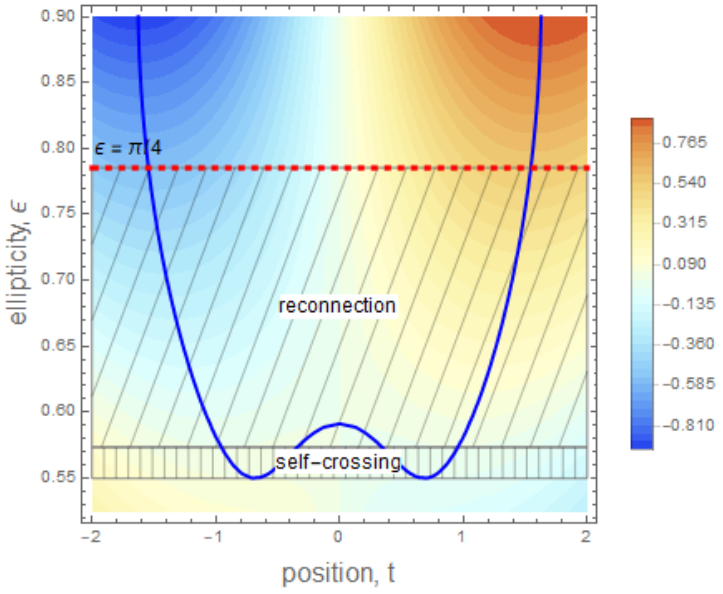

Figure 9: Phase diagram for $P = 0.2$. The blue line represents the curve along the extremum points; the red line $\epsilon = \pi/4 \approx 0.785$ is the ellipticity of the radially symmetric beam given for reference. The dashed regions represent the range of ellipticity at which reconnection or self-crossing is possible.

The blue line that represents the curve of extremum points appears to have quite a distinct shape which helps to identify the regions where reconnections or self-crossings can happen. For a fixed ϵ, the curve is anti-symmetric about the ψ_0-axis, meaning that a specific ϕ_c and t_c will yield the same result but on the other side of the beam in comparison to $-\phi_c$ and $-t_c$, as if the image is mirrored. From that, it is not hard to deduce that $t = 0$ is an inflection point for all values of ϵ and ϕ; and coincidentally, for every $t = 0$, $\phi = 0$ too.

Referring back to fig. 9, there are a few regions of interest in the diagram. They are divided into four: the lowest unlabeled region is where no reconnections happen outside of $t = 0$; the region where self-crossing can occur, labeled as "self-crossing" on the diagram; the region where reconnections happen only outside of $t = 0$; and the uppermost unlabeled region where the beam has a higher diffraction rate along the x-axis which depicts the annihilation points of the rings.

Firstly, there are no extremum points below $\epsilon = 0.549$. At such high ellipticity, the difference in diffraction rates is too large to sustain vertically aligned rings. Below is an example plot of vortex rings formed for ellipticity in that range. The only special point existing in that region is $t = 0$ where rings reconnect, forming a single merged ring.

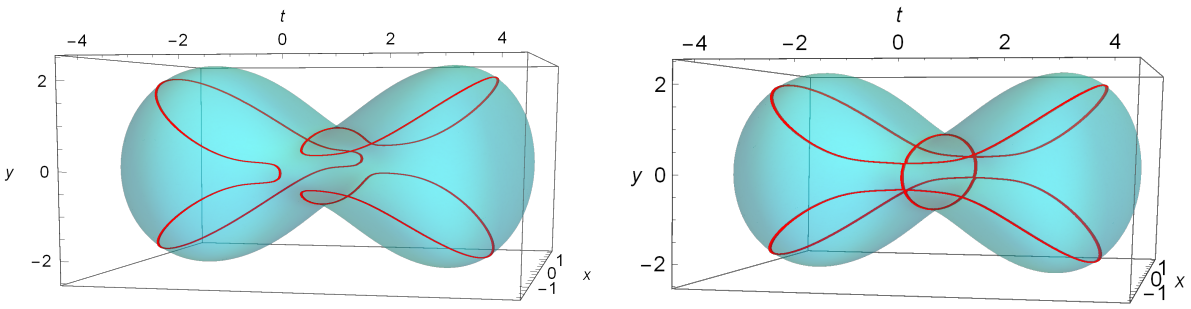

(a) $\phi = 0.031$ (b) $\phi = 0$

Figure 10: Vortex rings on spheroids for parameters $\epsilon = 0.540, P = 0.2$. a As expected, there are no reconnections. b Three rings merge into one single ring, the only setup where reconnections are possible at the given ellipticity range.

The reason why reconnections happen at $t = 0$ is related to the fact the beam is severely deformed. The rings at the right of fig. 10 can only be horizontally aligned, which makes reconnecting on $y = 0$ impossible. Despite that, due to the anti-symmetric nature of the phase eq. (3.9), there must exist a point where a single ring on the left and the two rings on the right switch places as ϕ change from a negative value to the positive one. Since the two rings have no possible way to be aligned vertically, the only way for them to "travel" to the left is to reconnect with the single ring and disconnect as ϕ changes. That is why, the only point that allows the reconnections is $t = 0$, which is exactly $\phi = 0$ as mentioned before.

The second region of interest is where self-crossings can happen ($0.549 < \epsilon < 0.578$), which is a very narrow range of ellipticities compared to the reconnection-only region, as shown in fig. 9. The lower bound of the region is obviously the lower bound of the extremum curve, while the upper bound of the region is located by finding ϵ at which the one set of the extremum points is at $\psi_0 = 0$.

The phase at fixed ϵ has two extremum points between the $0.549 < \epsilon < 0.591$. So intuitively, it might seem as if the upper limit for the self-crossing region is at $\epsilon = 0.591$, but the observations show otherwise. Referring back to fig. 9, the blue curve crosses the region four times. This means that there are four extremum points: a set of two points near $t = 0$ which I will call $T_1 = \{-t_1, t_1\}$ and a set of two outermost points $T_2 = \{-t_2, t_2\}$. T_1 plugged into fig. 3.11 will result in phase $|\phi_1|$, and T_2 will result in $|\phi_2|$. At $\epsilon = 0.578$, $|\phi_1| = |\phi_2|$. Below that range of ellipticity, $|\phi_1|$ has a higher value than $|\phi_2|$; and above that, $|\phi_1| < |\phi_2|$. That is the only feasible explanation as to why this relation makes $\epsilon = 0.578$ the upper limit for the self-crossing region.

The following plot provides an example of an obtained self-crossing ring.

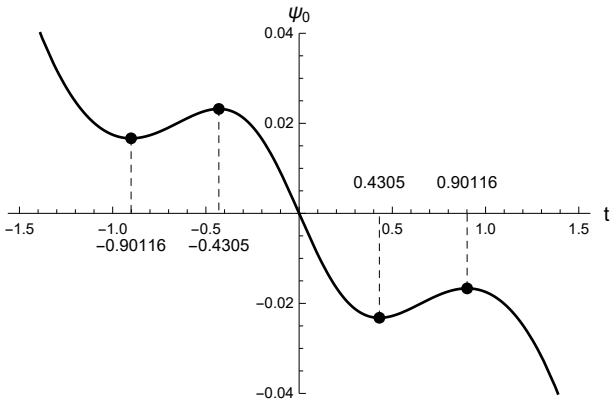

Figure 11: The phase at $y = 0$ ($\epsilon = 0.565, P = 0.2$). The dashed lines show the position of extremum points.

Since $|\phi_1| > |\phi_2|$, the self-crossing is possible. The points T_2 represent the coordinates after which the self-crossing starts to happen; $(-\phi_2, \phi_2)$ is the range between which the self-crossing happens. So it starts right after ϕ_2, peaks at ϕ_1, and collapses afterward. The following plots demonstrate the said phenomenon.

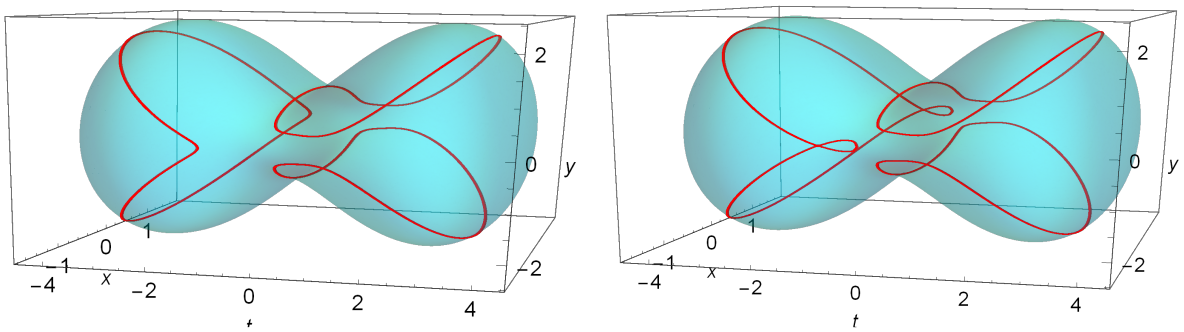

(a) $\phi = -0.0232$ (b) $\phi = -0.01667$

Figure 12: Vortex rings on spheroids for parameters $\epsilon = 0.565$ and $P = 0.2$. a The phase after which the self-crossing starts. b The phase at which self-crossing reaches its peak.

As expected, the self-crossing peaks at $\phi = -0.01667$ and does not start at exactly $\phi = -0.0232$. Moreover, by further varying ϕ, it can be observed that the reconnection happens at $t = 0$, similar to the cases in the previous region. The mechanism behind this phenomenon is the same; the rings are too deformed and must be reconnected and disconnected in order to switch places. However, unlike in the previous region, both self-crossing and reconnection can be observed simultaneously:

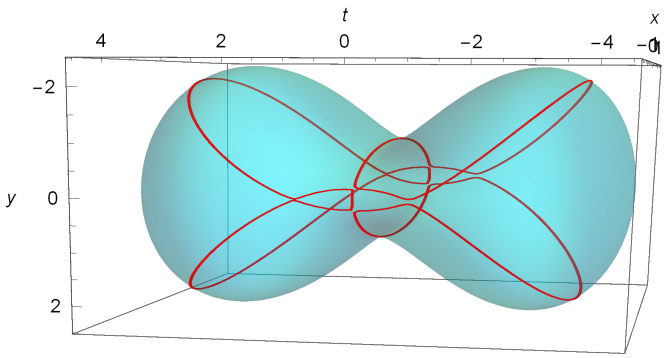

Figure 13: Vortex ring reconnection and self-crossing occurred simultaneously as $\phi = 0$, $\epsilon = 0.565$ and $P = 0.2$.

Moving to the next region, $0.578 < \epsilon < 0.785$, the set T_1 will be of no use, since no self-crossings are possible and only reconnections can happen in this region. Ellipticity within this given range allows for the rings to stay vertically oriented at smaller values of ϕ.

There are two different ranges of interest ($0.578 < \epsilon < 0.591$ and $0.591 < \epsilon < 0.785$), but observations show that they have no distinguishing traits. The reconnections happen at the corresponding $|\phi_2|$ within $0.578 < \epsilon < 0.591$, $|\phi_1|$ has no effect on reconnections; and within $0.591 < \epsilon < 0.785$ there is only one set of extremum points.

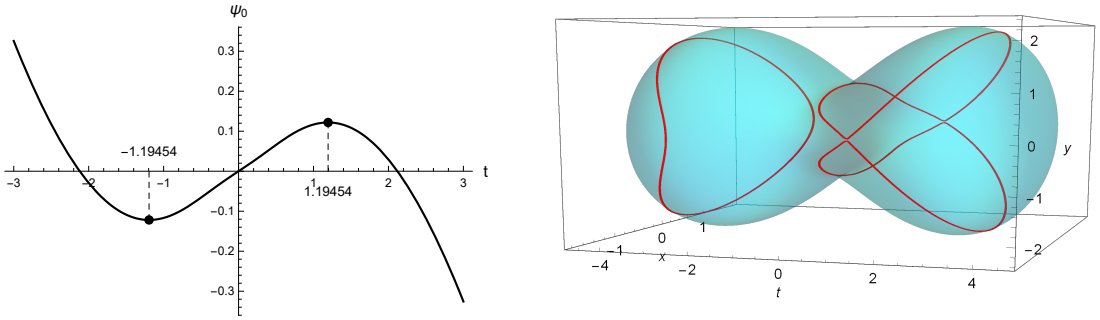

(a) Phase at $y = 0$ (b) Ring reconnections

Figure 14: a Phase equation (3.11) plotted for $\epsilon = 0.628, P = 0.2$. The dashed lines show the positions of extremum points. b Resulting vortex rings reconnection occurred at $\phi = 0.1218$.

Moving onto the last region, there are no possible reconnections above $\epsilon = 0.785$, even though the extremum points exist. Recalling fig.4b, the ellipticities above $\epsilon = 0.785$ mean that the diffraction rate is now higher in x-direction. Nevertheless, by tracing the parameters at the extremums, the ring annihilation points can be found. The following plot demonstrates the said phenomenon:

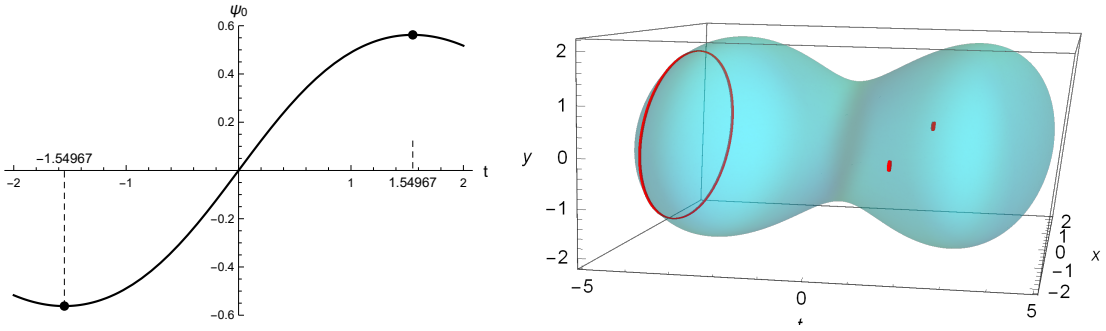

(a) Phase at $y = 0$ (b) Ring annihilation

Figure 15: a Phase equation (3.11) plotted for $\epsilon = 0.790, P = 0.2$. The dashed lines show the positions of extremum points. b Resulting vortex rings annihilation at $\phi = 0.5621$.

As predicted, at a specific t_c and ϕ_c, the two rings annihilate. Beyond that, only a single ring will be left, which will also be annihilated as ϕ varies further.

4 CONCLUSION

The shape and locations of the vortex rings formed as a result of the interference of the elliptical Gaussian beam and the plane wave are determined by three parameters: the relative amplitude P, the phase difference ϕ, and the ellipticity of the beam ϵ. The rings formed using the radially symmetric Gaussian beam were governed only by two parameters P and ϕ, however, they cannot reconnect. This proves that ellipticity is the single major factor that determines the reconnections, as the difference in diffraction rates along x- and y-axes deform the rings to various extents, depending on the parameter ϵ. The higher the ellipticity, the stronger the deformation, which results in intricate reconnection patterns.

The two types of reconnections were identified: reconnections that merge the rings together and the self-crossing of a single ring. At different ellipticity ϵ, the types of reconnections would vary, and so to pinpoint which range of ellipticities causes a specific type of reconnection, the phase profile was analyzed. It was uncovered that at a fixed ϵ, the reconnections happen at the extremum points of the phase $\psi(t)$.

By further analyzing the extremum points, I identified that at the ranges of ϵ closer to $\pi/4$, which corresponds to the radially symmetric beam, the two rings reconnect outside of the $t = 0$ point. No self-crossings happen at this range. The reconnected rings then merge, and as ϕ varies, they disconnect and form two separate rings. At higher ellipticities, a very narrow range of ϵ allows for the self-crossings, where a single ring deforms and creates a loop-like structure at ϕ very close to 0. The reconnections at this range and beyond only happen at $\phi = 0$, which is exactly at $t = 0$, and in this case, all three rings reconnect. After a certain ϵ, no reconnections are possible.

The whole system is symmetric, meaning that at a certain ϕ the resulting rings will be the same as for $-\phi$, with the only difference - the image will be mirrored. The symmetry is potentially the reason why no knots appear, since by varying the parameters the rings only reconnect and disconnect. Our next objective is to introduce asymmetry to the system and investigate the response of reconnections to it.

The plan is to replicate the same procedure using an astigmatic beam. In the astigmatic beam, the focal points for the x- and y-components of the beam do not coincide, causing the asymmetry, which is not present in the current setup. Previous research has indicated that the presence of beam rotation leads to the appearance of vortex knots, so after observing the effects of astigmatism, the next step is to introduce the case of the rotating beam.

While it cannot be guaranteed that the introduction of rotation will result in the appearance of vortex knots, it is still important to recognize that the mechanisms underlying knotting are far more intricate than previously thought. Having a system that forms knots by varying a certain number of parameters may sound too idealistic, however, even if knotting will not happen when the symmetry is broken, it can still provide valuable insights into the underlying mechanisms.

Nevertheless, the fact that a system as simple as the one governed by only three parameters can result in vortex reconnections is already intriguing.

REFERENCES

[1] D. Raymer and D. Smith, "Spontaneous knotting of an agitated string," Proceedings of the National Academy of Sciences **104**, 16432–16437 (2007).

[2] M. Berry, "Making waves in physics," Nature **403**, 21 (2000).

[3] R. Cooper, M. Mesgarnezhad, A. Baggaley, and C. Barenghi, "Knot spectrum of turbulence," Scientific Reports **9**, 10545 (2019).

[4] R. Ricca, "Applications of knot theory in fluid mechanics," Banach Center Publications **19**, 013001 (1998).

[5] M. Berry and M. Dennis, "Knotted and linked phase singularities in monochromatic waves," Proceedings of the Royal Society of London A **457**, 2251 (2001).

[6] J. Leach, M. Dennis, J. Courtial, and M. Padgett, "Vortex knots in light," New Journal of Physics **7**, 55 (2005).

[7] J. Zhong, S. Liu, X. Guo, P. Li, B. Wei, L. Han, S. Qi, and J. Zhao, "Observation of optical vortex knots and links associated with topological charge," Optics Express **29**, 38849 (2021).

[8] L. Kong, W. Zhang, P. Li, X. Guo, J. Zhang, F. Zhang, J. Zhao, and X. Zhang, "High capacity topological coding based on nested vortex knots and links," Nature Communications **13**, 2705 (2022).

[9] J. Nye, *Natural focusing and fine structure of light: caustics and wave dislocations* (Institute of Physics Publishing, Bristol, 1999).

[10] O. Heaviside, *Electromagnetic theory, Volume 3* (Chelsea Publishing Company, New York, 1971).

[11] A. Desyatnikov, D. Buccoliero, M. Dennis, and Y. Kivshar, "Spontaneous knotting of self-trapped waves," Scientific Reports **2**, 771 (2012).

[12] C. Huygens, *Treatise on light* (Pieter van der Aa, Leiden, 1960).

[13] A. Einstein, "On the quantum theory of radiation," Physikalische Zeitschrift **18**, 121 (1917).

[14] T. Maiman, "Stimulated optical radiation in ruby," Nature **187**, 493 (1960).

[15] A. Schawlow and C. Townes, "Infrared and optical masers," Physical Review **112**, 1940 (1958).

[16] N. Basov and A. Prokhorov, "Theory of the molecular generator and molecular power amplifier," Soviet Physics Journal of Experimental and Theoretical Physics **3**, 560 (1956).

[17] J. Hecht, *Beam: the race to make the laser* (Oxford University Press, New York, 2005).

[18] J. Gordon, H. Zeiger, and C. Townes, "The maser - new type of microwave amplifier, frequency standard, and spectrometer," Physical Review **99**, 1264 (1955).

[19] J. Nishizawa, "Extension of frequencies from maser to laser," Proceedings of the Japan Academy, Series B **85**, 454 (2009).

[20] A. Siegman, "Unstable optical resonators for laser applications," Proceedings of the IEEE **53**, 277 (1965).

[21] A. Siegman, *Lasers* (University Science Books, Palo Alto, 1986).

[22] J. Foley and E. Wolf, "Note on the far field of a Gaussian beam," Optical Society of America **69**, 761 (1979).

[23] H. Kogelnik, "On the propagation of Gaussian beams of light through lenslike media including those with a loss or gain variation," Applied Optics **4**, 1562 (1955).

[24] J. Durnin, "Exact solutions for nondiffracting beams. I. The scalar theory," Optical Society of America **4**, 651 (1987).

[25] M. Dennis, Y. Kivshar, M. Soskin, and G. Swartzlander Jr, "Singular Optics: more ado about nothing," Journal of Optics A: Pure and Applied Optics **11**, 090201 (2009).

[26] A. Desyatnikov, L. Torner, and Y. Kivshar, *Progress in optics, Volume 47*, edited by E. Wolf (Cambridge University Press, Cambridge, 1999).

[27] J. Nye and M. Berry, "Dislocations in wave trains," Proceedings of the Royal Society of London A **336**, 165 (1974).

[28] V. Bazhenov, M. Vasnetsov, and M. Soskin, "Laser beams with screw dislocations in their wavefronts," Optical and Quantum Electronics **24**, 951 (1990).

[29] G. Bogatyrova, C. Fel'de, P. Polyanskii, S. Ponomarenko, M. M. Soskin, and E. Wolf, "Partially coherent vortex beams with a separable phase," Optics Letters **28**, 878 (2003).

[30] Y. Izdebskaya, T. Lu, D. Neshev, and A. Desyatnikov, "Dynamics of three-Airy beams carrying optical vortices," Applied Optics **53**, 248 (2014).

[31] B. Terhalle, T. Richter, A. Desyatnikov, D. Neshev, W. Krolikowski, F. Kaiser, C. Denz, and Y. Kivshar, "Observation of multivortex solitons in photonic lattices," Physical Review Letters **101**, 013903 (2008).

[32] A. Volyar, V. Shvedov, T. Fadeyeva, A. Desyatnikov, D. Neshev, W. Krolikowski, and Y. Kivshar, "Generation of single-charge optical vortices with an uniaxial crystal," Optics Express **14**, 3724 (2006).

[33] M. Soskin, S. Boriskina, Y. Chong, M. Dennis, and A. Desyatnikov, "Singular optics and topological photonics," Journal of Optics **19**, 010401 (2017).

[34] H. Rubinsztein-Dunlop *et al.*, "Roadmap on structured light," Journal of Optics **19**, 013001 (2017).

[35] A. Askin, "Acceleration and trapping of particles by radiation pressure," Physical Review Letters **24**, 156–159 (1970).

[36] K. Dholakia and T. Cizmar, "Shaping the future of manipulation," Nature Photonics **5**, 335 (2011).

[37] M. Padgett and R. Bowman, "Tweezers with a twist," Nature Photonics **5**, 343 (2011).

[38] M. Soskin and M. Vasnetsov, *Progress in optics, Volume 42*, edited by E. Wolf (North-Holland Publishing Company, Amsterdam, 2001).

[39] V. Kotlyar and A. Kovalev, "Controlling orbital angular momentum of an optical vortex by varying its ellipticity," Optics Communications **410**, 202 (2018).

[40] V. Kotlyar, A. Kovalev, and A. Porfirev, "Elliptic Gaussian optical vortices," Physical Review A **95**, 053805 (2017).

[41] C. Wan, Q. Cao, J. Chen, A. Chong, and Q. Zhan, "Toroidal vortices of light," Nature Photonics **16**, 519–522 (2022).

[42] M. Berry and M. Dennis, "Knotting and unknotting of phase singularities: Helmholtz waves, paraxial waves and waves in 2 + 1 spacetime," Journal of Physics A: Mathematical and general **34**, 8877 (2001).

[43] M. Dennis, R. King, B. Jack, K. O'Holleran, and M. Padgett, "Isolated optical vortex knots," Nature Physics **6**, 118 (2010).

[44] A. Desyatnikov, D. Buccoliero, M. Dennis, and Y. Kivshar, "Suppression of Collapse for spiraling elliptic solitons," Physical Review Letters **104**, 053902 (2010).

[45] A. Desyatnikov, "Vortex rings in paraxial laser beams," Manuscript in preparation (2023).

[46] D. Andrews and M. Babiker, *The angular momentum of light* (Cambridge University Press, Cambridge, 2012).

[47] M. Born and E. Wolf, *Principles of optics* (Cambridge University Press, Cambridge, 1999).